JOURNAL OF MATERIALS SCIENCE 16 (1981) 465–476

Investigation into the effect of an increase in tungsten content on the behaviour during ageing of maraging type Fe-Ni-Co-W alloys

E. SAKR, C. SERVANT, P. LACOMBE
Laboratoire de Métallurgie Physique, associé au CNRS 177, Université de Paris-Sud, 91405 Orsay, France

In the present paper, the behaviour during ageing is compared in the temperature range 400 to 500° C of the three martensitic alloys Fe–18.5 wt % Ni–8.99 wt %Co–4.87 wt %W, Fe–17.5 wt % Ni–8 wt % Co–8 wt % W and Fe–17 wt % Ni–8 wt % Co–10 wt % W. The kinetics of precipitation were followed by hardness measurements and small-angle X-ray scattering and electron microscopy studies. The ageing effect can be observed in three successive stages. In the second stage,with which a marked increase of the hardness is associated, there is formation and growth of intermetallic precipitates of (Fe, Ni, Co)$_3$W ≡ A_3W. These precipitates are elongated ellipsoids, of several nanometres in length. The preferred direction of growth of these precipitates is ⟨1 1 1⟩ of the martensitic matrix and the orientation relationship with the martensitic matrix is $\{0\,1\,1\}_M // (0\,1\,0)_{A_3W}$ and $\langle 1\bar{1}1\rangle_M // [1\,0\,0]_{A_3W}$, identical to that found for the Ni_3Mo precipitate in the quaternary alloys of the same composition but with the W-content substituted for by Mo; but none of the three above-mentioned stages corresponds to the formation of ω-phase.

1. Introduction

In the temperature range 300 to 500° C a strengthening phenomenon occurs in the ternary alloys Fe–16.4 wt % Ni–8.2 wt % Mo and Fe–15.4 wt % Ni–10.2 wt % Mo and the quaternary alloy Fe–18.65 wt % Ni–8.99 wt % Co–4.87 wt % Mo of the maraging type. During isothermal ageing of such alloys a successive formation of Mo-rich clusters, a superstructure of type $A_8B \rightarrow A_7B_2$ (with A = Fe, Ni and Co and B = Mo), ω-phase of type A_2B and intermetallic compounds of type Ni_3Mo or σ-FeMo, followed by reversed austenite [1–7] have been found. In a previous paper [8], the effect is compared of Mo substituted by W on the ageing of the ternary alloy Fe–16.4 wt % Ni–8.2 wt % Mo. In this case, it is shown in particular that the ω-phase had not been observed. The same result was also obtained for the quaternary alloy Fe–18.5 wt % Ni–8.99 wt % Co–4.87 wt % W [9]. Hence the intermetallic compound formed, of the type A_3W (where A represents Fe, Ni, and Co) is identified as being isomorphous with Ni_3Mo [6]. The percentage weight of W in the quaternary alloy is increased in order to establish whether the ω-phase formation is related to this parameter.

The present publication yields the main conclusions of our study concerning the two alloys Fe–17.5 wt % Ni–8 wt % Co–8 wt % W and Fe–17 wt % Ni–8 wt % Co–10 wt % W and compares their behaviour with that of the quaternary alloy Fe–18.5 wt % Ni–8.99 wt % Co–4.87 wt % W during isothermal ageing.

2. Experimental procedure

2.1. Preparation and structure of the alloys

The two alloys concerned in this work are Fe–17.5 wt % Ni–8 wt % Co–8 wt % W and Fe–17 wt % Ni–8 wt % Co–10 wt % W and will be referred to as Alloys 2 and 3 respectively, while the previously studied alloy Fe–18.5 wt % Ni–8.99 wt % Co–4.87 wt % W will be referred to as Alloy 1. The three alloys have been prepared from mixtures of high purity powders by solid-

0022–2461/81/020465–12$03.20/0

state sintering processes. The Fe and Ni powders were of ex-carbonyl origin; the Co and W powders were obtained by the reduction of CoO_3, MoO_3 and WO_3 by H_2. The green pellets were compressed under a pressure of 5 tons cm^{-2} and then sintered at 1400° C for 4 h.* The samples were rolled to the required thickness using intermediate anneals at 1400° C for 4 h and cooled to room temperature at an average rate of 600° Ch^{-1}. Alloys 2 and 3 consisted of a single phase (body-centred cubic, lath martensite) and were homogeneous on the scale of the microprobe.

2.2. Experimental methods

The dilatometric analyses were carried out with a DHT 60 type differential dilatometer. In this apparatus, the length of the sample is continuously compared with a standard alumina sample. The K magnification coefficient was equal to 1530 and the dimensions of the samples were 20 mm × 4 mm × 1.5 mm [2]. The average heating and cooling rates were 300 and 450° Ch^{-1}, respectively.

The microhardness measurements were performed at room temperature under a load of 300 g, on samples 10 mm × 4 mm × 3 mm. These samples were previously aged in a DITIRC dilatometer [10]. With this apparatus, the time to reach the ageing temperature was very short (between 1 and 2 min at 450° C). For each hardness value plotted, twenty measurements were taken.

The electron microscope examinations were carried out with a JEOL 100C at 100 kV. Thin foils were obtained by anodic dissolution at 20 V in a bath containing: 100 g chromic anhydride, 540 cm^3 acetic acid (density = 1.33) and 30 cm^3 distilled water.

Standard geometric and crystallographic conditions were used to estimate the size of the precipitates and are given in Section 3.3.

2.3. Small-angle X-ray scattering

A standard convergent type, central scattering apparatus was used, associated with a GS 2000 type CGR-diffractometer (using the step procedure). The X-ray beam was limited by tantalum slits adjusted to 100 ± 1 μm. The monochromatic X-ray radiation ($\lambda_{K\alpha_1}$, Mo = 0.709 Å) used was considered as linear and infinite [11]. Any variations in the direct beam intensity were recorded by a scintillation counter, which was positioned at the angular value of the martensite diffraction line, {1 1 0}, of the two alloys. The intensity scattered by the heterogeneities of electron densities is expressed as the difference between the intensities of the radiation scattered by the aged and unaged samples corrected for absorption. By comparison with direct beam intensity I_0, the measurements of the scattered intensity become quantitative. Foils of 40 μm thickness were used.

3. Results and discussion

3.1. Comparison of the behaviour of alloys 1, 2 and 3 during anisothermal heating

During the course of a simple cycle consisting of heating at an average rate of 300° Ch^{-1} between

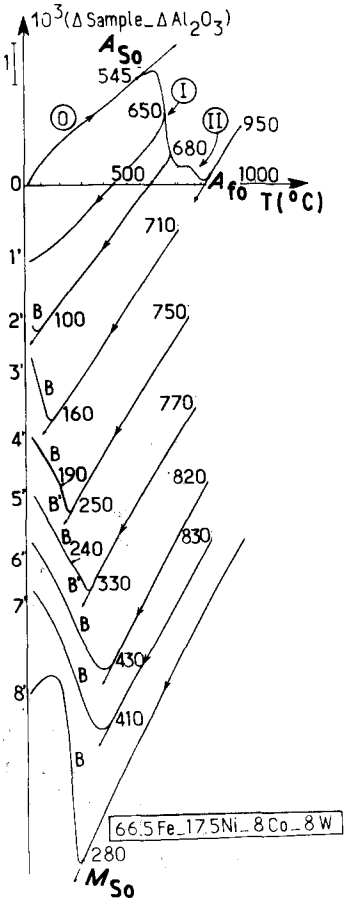

Figure 1 Dilation curves for Alloy 2 recorded during heating up to 950° C then cooling from different temperatures (T_C) in the austenitic transformation range.

*The heat treatments for preparation and homogenization of the alloys, the anisothermal and isothermal anneals were carried out under purified hydrogen.

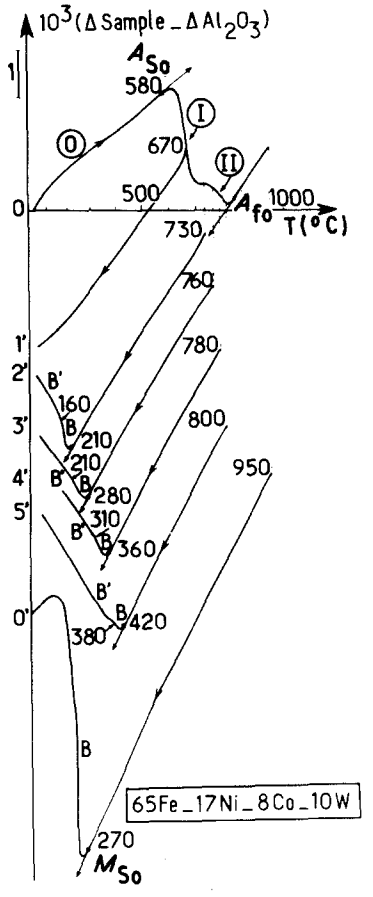

Figure 2 Dilation curves for Alloy 3 recorded during heating up to 950° C, then cooling from different temperatures (T_C) in the austenitic transformation range.

20 and 950° C, and cooling at an average rate of 450° Ch^{-1}, the behaviour of these three alloys is similar. In fact, from the dilatometric curves of heating shown in Figs 1 and 2, it appears that the martensite → austenite transformation occurs between the A^*_{So} and A^*_{fo} points in two distinct steps, designated by I and II, which both represent contractions.

The curves obtained by cooling from 950° C show that the M_{So} point which indicates the beginning of the austenite → martensite transformation slightly decreases when the W content increases.

The curves obtained by cooling from the critical temperatures, T_C, ranging between the two points A_{So} and A_{fo} give the same results as those previously published for Alloy 1, that is one of the following:

(a) no M_S point (curve 1', Figs 1 and 2) and the austenite formed between A_{So} and T_C was stable down to room temperature;

(b) two successive M_S points corresponding to the transformation $\gamma \rightarrow M$ in two successive stages designated by B and B', see Figs 1 and 2, curves 2', 3', 4' and 5'.

These results show that during the course of heating between 20° C and A_{So}, the martensite with concentration of (Ni + W) = Co "ages" progressively and decomposes into zones which are respectively enriched in (Ni + W), designated as M_R, and depleted in (Ni + W), designated as M_P. The M_R martensite transforms into austenite by a predominantly diffusional mechanism during Step I while the M_P martensite transforms during Step II according to the following process

$$\begin{aligned} M_R &\rightarrow M_{RP} + \gamma_{RR}; \\ M_P &\rightarrow M_{PP} + \gamma_{PR}. \end{aligned} \qquad (1)$$

Therefore during the course of cooling from T_C, the γ_{RR} and γ_{PR} austenites may or may not transform into two distinct martensites at the M_{S_P} and M_{S_R} points, depending upon their composition. When T_C approaches the A_{fo} point the compositions of the two austenites tend to homogenize and only one M_S point is observed during cooling, see Fig. 1, curves 6' and 7'.

The formation of compositional heterogeneities during heating and their growth is clearly revealed during isothermal ageing tests.

3.2. Study of the precipitates formed during isothermal ageing

From the hardness measurements, three successive stages could be observed during isothermal ageing, see Figs 3 and 4 as for Alloy 1, [9]. Stage I which occurs during the early stages of ageing (i.e. up to about 15 min) and exhibits an increase in the hardness followed by a plateau. This increase is approximately the same and equal to about 60 HV, whatever the ageing temperature in the range 400 to 480° C and for either tungsten content of the alloy. It has been shown by electron microscopy that Stage I does not correspond to the formation of the ω-phase and by analogy with the Mo alloys may correspond to the formation and growth of W-clusters in the martensitic matrix. Stage II, which exhibits a larger increase in the hardness

*The subscript 'o' is used to avoid confusion with the different A_S and M_S points obtained during the thermal cycles which were interrupted at some temperature T_C between the A_{So} and A_{fo} points.

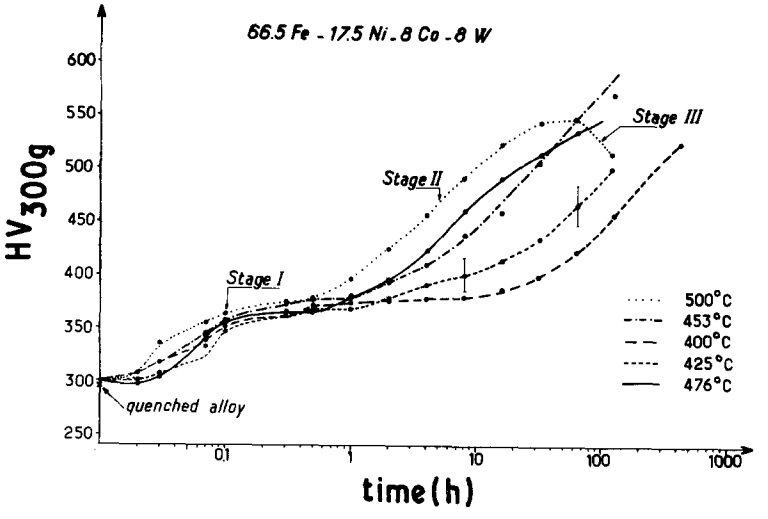

Figure 3 Hardness curve for Alloy 2.

than that observed for Stage I, begins at a time which decreases as the ageing temperature increases, it corresponds to the formation and growth of precipitates which have been studied by both electron microscopy and small-angle scattering of X-rays (see Sections 3.3 and 3.4). Stage III which shows a marked decrease in the hardness and reveals the formation of the reversed austenite.

For Stage II only, it has been shown that the kinetics of precipitation fits well with the Johnson–Mehl equation [12]

$$y(t) = 1 - \exp[-(kt)^n], \qquad (2)$$

where $y(t)$ represents the fraction transformed after a time t and is equal to $[H(0) - H(t)]/[H(0) - H(\infty)]$. $H(0)$, $H(t)$ and $H(\infty)$ respectively correspond to the value of the hardness at times $t = 0$, $t = t$ and $t = \infty$.

For both Alloys 2 and 3 in the temperature range 400 to 500° C it was found that the values of n and K vary between 0.8 and 1 and between 0.004 and 0.16 h^{-1}, respectively.

This value of unit for n should correspond to the diffusion-controlled growth of rods along their axes [12]. In fact, it is noted in Section 3.3. that during ageing, by using the electron microscope, the growth of precipitates which are elongated ellipsoids rather than rods is observed.

Assuming that the rate of precipitation is equal to

$$\frac{dy}{dt} = A \exp\left(-\frac{Q}{RT}\right), \qquad (3)$$

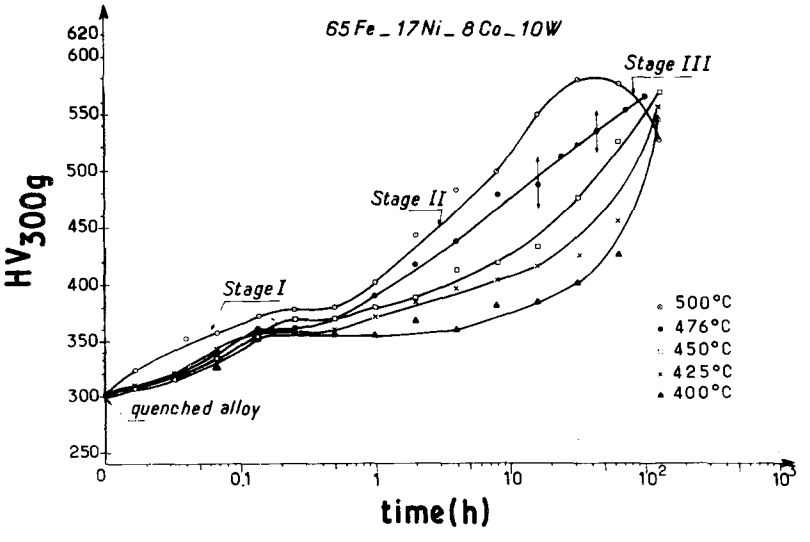

Figure 4 Hardness curve for Alloy 3.

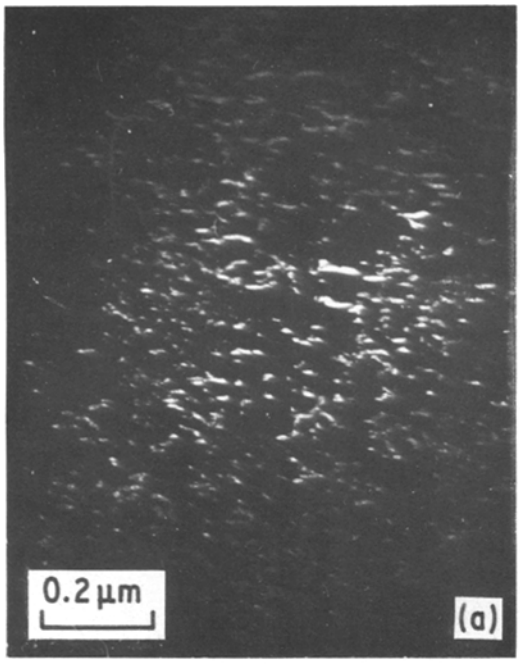

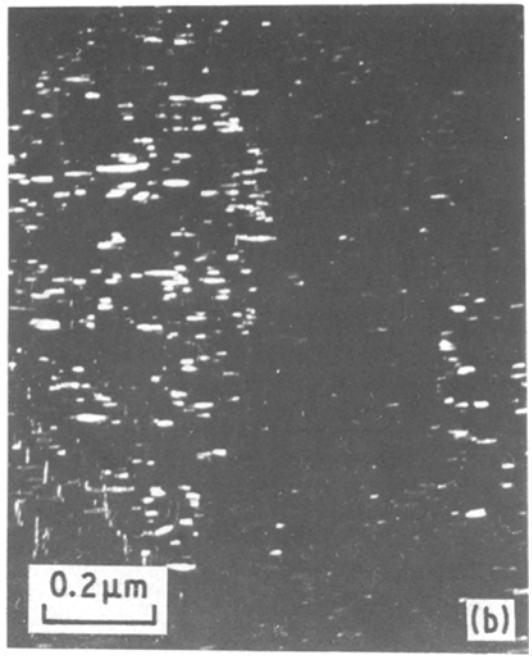

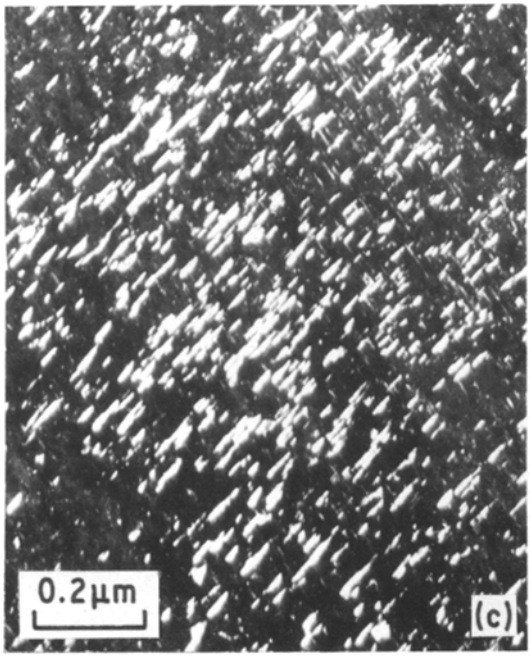

Figure 5 Dark-field micrographs obtained on Alloy 3 aged for (a) 20 h, (b) 50 h and (c) 120 h at 450° C, from the spot (0 0 2) of the precipitates on the section of the martensitic matrix of zone axis $\langle 1\ 1\ 0 \rangle_M$.

where A is a constant independent of the temperature and Q is the apparent activation energy of precipitation which was calculated for various values of the transformed fraction $y(t)$ varying from 0.05 to 0.95, it was found that Q is approximately constant and equal to 146 kJ mol^{-1}.

This value, which is lower than that (293 kJ mol^{-1}) obtained for volume diffusion of ^{185}W in b c c iron [13], may suggest that the growth of precipitates occurs by a pipe diffusion phenomenon as was observed for Alloy 1 [9].

3.3. Studying of stage II by electron microscopy

In the temperature range of interest, we have observed from the study of diffraction patterns and bright- and dark-field micrographs, the formation and growth of precipitates with the same nature and form as have already determined in the case of Alloy 1 [9]. These precipitates have the chemical formula A_3W (where A represents the elements Fe, Ni and/or Co) and refer to the preferred direction of growth $\langle 1\ 1\ 1 \rangle_M$. Fig. 5a, b and c shows the dark-field micrographs obtained for Alloy 3 aged for 20, 50 and 120 h, respectively.

It is found that: (a) Some of the precipitates seem to be rod-shaped but, in fact, an examination at higher magnification shows the resolution of these rods into smaller, definitely less elongated particles (as illustrated in Fig. 6) and, therefore, these precipitates are rather elongated ellipsoids of revolution, the axes of which have the dimensions: $2a$, $2a$ and $2\nu a$; (b) The precipitates present a fair size distribution; (c) The growth of the precipitates,

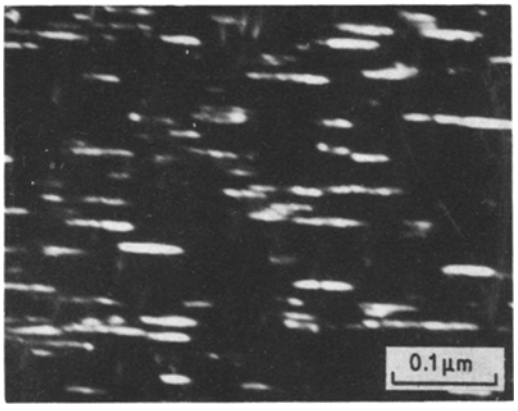

Figure 6 Dark-field micrograph obtained at a higher magnification than Fig. 5, showing that the precipitates are elongated ellipsoids rather than rods.

which is observed in the direction ⟨1 1 1⟩ of the martensitic matrix, is a function of the ageing time.

The projected dimensions of the precipitates were measured by electron microscopy. Taking into account that the preferred direction of growth of the precipitates is ⟨1 1 1⟩ martensite, it is convenient to observe them firstly in a section of matrix with zone axis $\langle 1\ 1\ 0\rangle_M$ and secondly always obtained for the same tilt angle τ_x (on choosing $\tau_x = 0$) and thirdly with the same diffraction spot. For example, for a section with zone axis $\langle 1\ \bar{1}\ 0\rangle_M$ where the precipitates, which are elongated according to the directions $\langle 1\ 1\ 1\rangle_M$ and $\langle \bar{1}\ \bar{1}\ 1\rangle_M$ are observed in real dimensions, the precipitates elongated in the directions $\langle 1\ \bar{1}\ 1\rangle_M$ and $\langle \bar{1}\ 1\ 1\rangle_M$ and have a length which is equal to their real length $(X \cos \rho_{\langle 1\bar{1}1\rangle,\langle 1\bar{1}0\rangle})$. From numerous dark-field micrographs with the geometric and crystallographic conditions indicated above, the average and maximum values of the long and short axes of the ellipsoids and then the value ν of the ratio of those axes for different ageing times at 450° C could be estimated, as shown in Table I.

The experimental diffraction patterns with zones axes $\langle 1\ 1\ 0\rangle_M$ and $\langle 1\ 1\ 3\rangle_M$ of the martensitic matrix are shown in Figs 7a and 8a, respectively. If these patterns are compared with those obtained for the same zone axes of the martensitic matrix but from the ω-phase of the alloys Fe–18.65 wt% Ni–8.99 wt% Co–4.87 wt% Mo (Figs 7b and 8b), in the two cases, spots of diffraction given by the precipitates in the matrix at 1/3 and 2/3 of $\langle 2\ 1\ 1\rangle^*_M$ which could suggest the presence of ω-phase in the alloys with W are noted. But the construction of the stereographic projection of the studied martensitic lath and, in particular, the investigation of sections with the zone axis $\langle 1\ 0\ 0\rangle_M$ allows us to remove an ambiguity and to conclude the unique presence of intermetallic compounds A_3W in the alloys with W. In Figs 9 and 10, the theoretical diffraction patterns with the zone axes $\langle 1\ 1\ 0\rangle_M$ and $\langle 1\ 1\ 3\rangle_M$ are shown, calculated according to the procedure in [9] and from the following orientation relationship with the martensitic matrix:

$$\begin{aligned} \{0\ 1\ 1\}_M &/\!/ (0\ 1\ 0)_{A_3W} \\ \langle 1\ \bar{1}\ 1\rangle_M &/\!/ [1\ 0\ 0]_{A_3W}. \end{aligned} \qquad (4)$$

Comparison of theoretical and experimental diffraction patterns shows, in the same selected area, the twelve theoretical families of precipitates that result in twelve variants of the orientation relationship, Equation 4. In fact, only eight families can easily be observed, owing to the relative intensity of diffraction spots for certain numbers of these families.

In the construction of theoretical diffraction patterns which result from the superimposition of reciprocal lattice sections of the martensite and those of the possible twelve families of precipitates (when the precipitates and matrix meridians are not coinciding) it is important to emphasize that sometimes there are ambiguities concerning the choice of the nearest precipitate meridian to the matrix meridian. It is often preferable to choose a precipitate meridian which is not so near that of the matrix, but on which there are poles of planes with small indices. These planes have large lattice spacings which give

TABLE I

Ageing time (h)	Major axis		Minor axis		ν	
	$\bar{L}$ (Å)	L_{max} (Å)	$\bar{l}$ (Å)	l_{max} (Å)	$\bar{\nu}$	ν_{max}
20	160	440	80	110	2	4
50	185	500	80	110	2.3	4.5
120	210	610	80	110	2.6	5.5

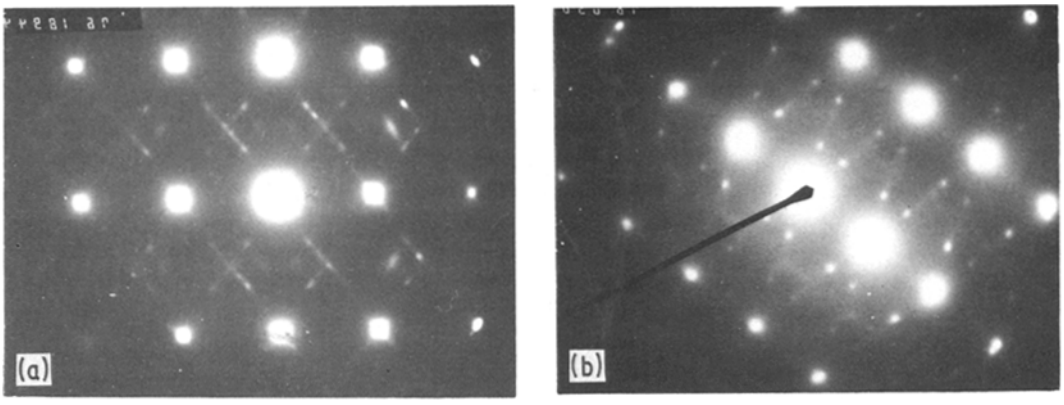

Figure 7 Experimental diffraction patterns with the zone axis $\langle 1\,1\,0\rangle_M$ obtained (a) for Alloy 3 aged for 120 h at 450° C and (b) for Fe–18.65 wt % Ni–8.99 wt % Co–4.87 wt % Mo aged for 15 h 50 min at 414° C.

diffraction spots near enough to the centre and hence they are better observed experimentally.

The theoretical diffraction patterns are in good agreement with those obtained experimentally and the spots on the latter could be explained by diffraction, either simple or multiple.

However, on the experimental diffraction patterns parasitic spots are often observed owing to the fact that diffraction occurs at the edge of the thin foil which has a certain curvature.

Fig. 11 shows a dark-field micrograph obtained for Fe–18.65 wt % Ni–8.99 wt % Co–4.87 wt % W aged for 120 h at 454° C. Comparison between this figure and Fig. 5c indicates that the quantity of A_3W precipitates increases with the W content in the alloy for the same temperature and the same period of ageing.

3.4. Study of precipitation by small-angle scattering of X-rays

Figs 12 and 13 represent the small-angle X-ray scattering curves as a function of time for Alloys 1 and 3 both aged at 450° C. The curves corresponding to the second stage of ageing only are shown. Two points should be noticed from these figures. (a) The scattering intensity decreases in a monotonic way with increasing s (the scattering vector) and no modulation, such as that produced by interference between the waves scattered by the base Mo precipitates, with an approximately regular distribution in the quaternary alloy with Mo (average distance between precipitates $d = 1/s \simeq 120$ Å) is observed for these quaternary alloys with W; the same monotonic decrease of the scattered intensity against s was observed in the case of the ternary alloys with W [8]. (b) For an identical and small s value, firstly, the $j_n(s)$ values increase as the ageing time increases up to 120 h, so the formation of the reversed austenite has not yet begun (in fact, when this last phenomenon occurs, $j_n(s)$ should decrease because the γ phase of reversion which is formed consecutively to the

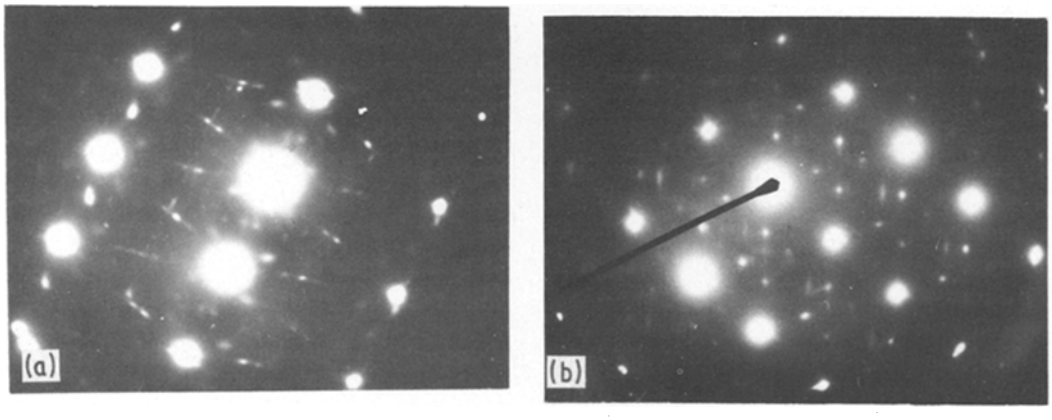

Figure 8 Experimental diffraction patterns with the zone axis $\langle 1\,1\,3\rangle_M$ obtained (a) for Alloy 3 aged for 120 h at 450° C and (b) for Fe–18.65 wt % Ni–8.99 wt % Co–4.87 wt % Mo aged for 15 h 50 min at 414° C.

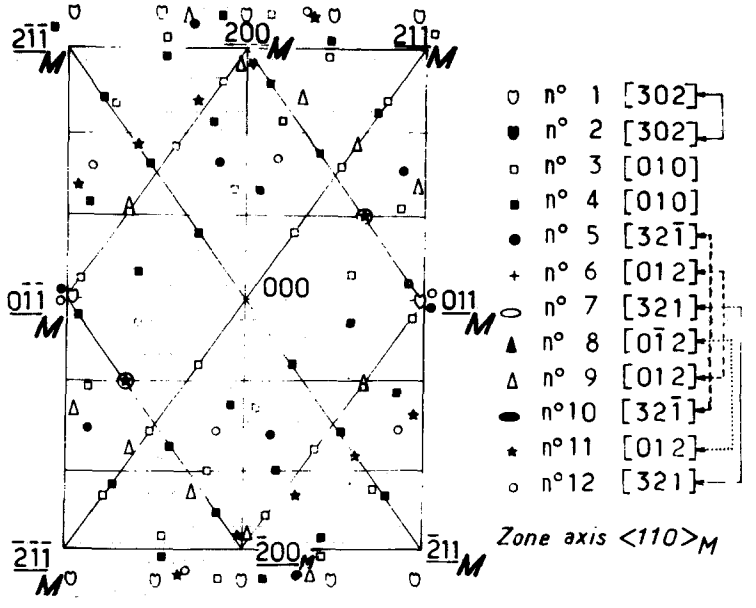

Figure 9 Theoretical diffraction patterns of the twelve families of precipitates for the zone axis of the martensitic matrix $\langle 1\,1\,0\rangle_M$. The families which are superimposed are connected by arrows.

reversal of the precipitates into the martensitic matrix, has a composition somewhat identical to that of the martensite; furthermore, the electron microscopic examination reveals that an infinitesimally small quantity of γ is formed after an ageing of 120 h) and, secondly, the $j_n(s)$ values are greater when the W content of the alloy is higher.

3.5. Determination of the R_G Guinier radius

The calculation of the gyration radius depends on the hypothesis of identical particles (same nature, same form, same dimensions) which are widely enough separated in a system and taking all possible orientations in order that the interparticle interferences will be negligible [11].

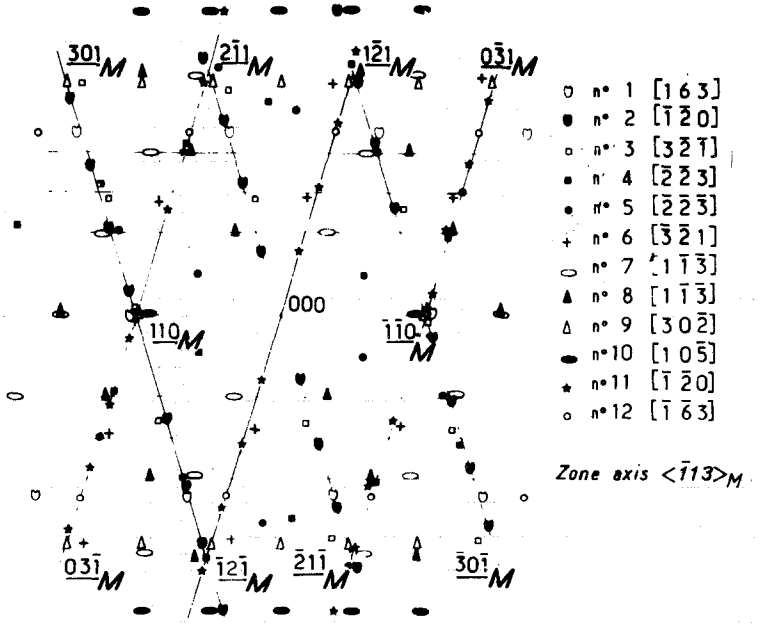

Figure 10 Theoretical diffraction patterns of the twelve families of precipitates for the zone axis of the martensitic matrix $\langle 1\,1\,3\rangle_M$.

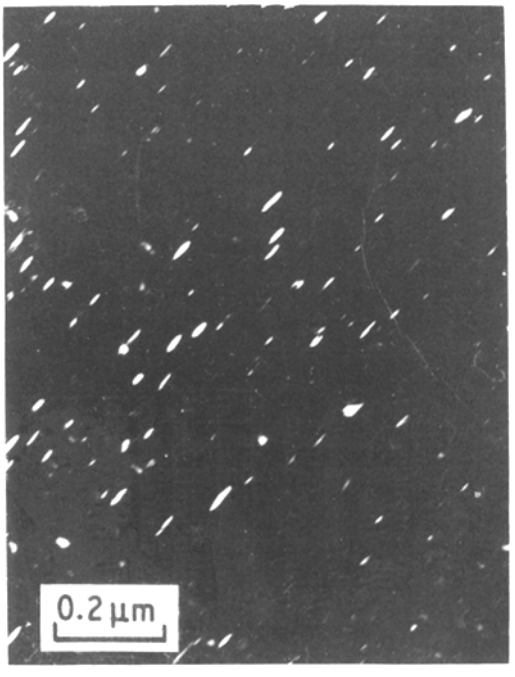

Figure 11 Dark-field micrograph obtained for Alloy 1, aged for 120 h at 450° C.

In this case, the precipitates have an orientation relation, Equation 4, with respect to the martensitic matrix. Nevertheless, considering the small size of the martensitic laths (which are disoriented between them) compared with the volume of the sample bathed by the X-ray beam, it may be considered that in the sample which is an isotropic polycrystal, the precipitates do not present the preferred orientation. The estimation made on the dark-field electron micrographs of the volume occupied by the precipitates of the twelve families shows that this volume does not exceed 15% of the sample volume.

The $\log j_n(s) = f(s^2)$ curves in Figs 12 and 13 show a curvature in the whole of the domain in which they are traced. This confirms the size distribution of the precipitates observed by electron microscopy.

We calculated the gyration radius of precipitates for the very steep slope of the curve $\log j_n(s) = f(s^2)$ which is still lower than that of the biggest precipitates existing in the sample. Fig. 14 shows the evolution of gyration radius as a function of ageing time for the three alloys. It has been indicated in Table II, for Alloy 3, that the dimensions of $2R_G$ and $2\nu R_G$ of the ellipsoids of revolution representing the precipitates where R_G (the Guinier radius) is equal to half the minor axis of the ellipsoid $\{R_G = [5/(2+\nu^2)]^{1/2} R_G\}$. ν was estimated from the dark-field electron micrographs. The curve $\nu = f(t)$ was traced and for the very short ageing time, ν was obtained by extrapolation. It was noted that the gyration radius of precipitates increases with the weight of W in the alloy, quite rapidly in the first hours of ageing. Otherwise the Guinier radius of the greatest accessible precipitates, from the scattering curve and calculated from R_g and the estimation of ν obtained by electron microscopy remained constant. This fact justifies the hypothesis that the growth of the precipitates follows the large axis of

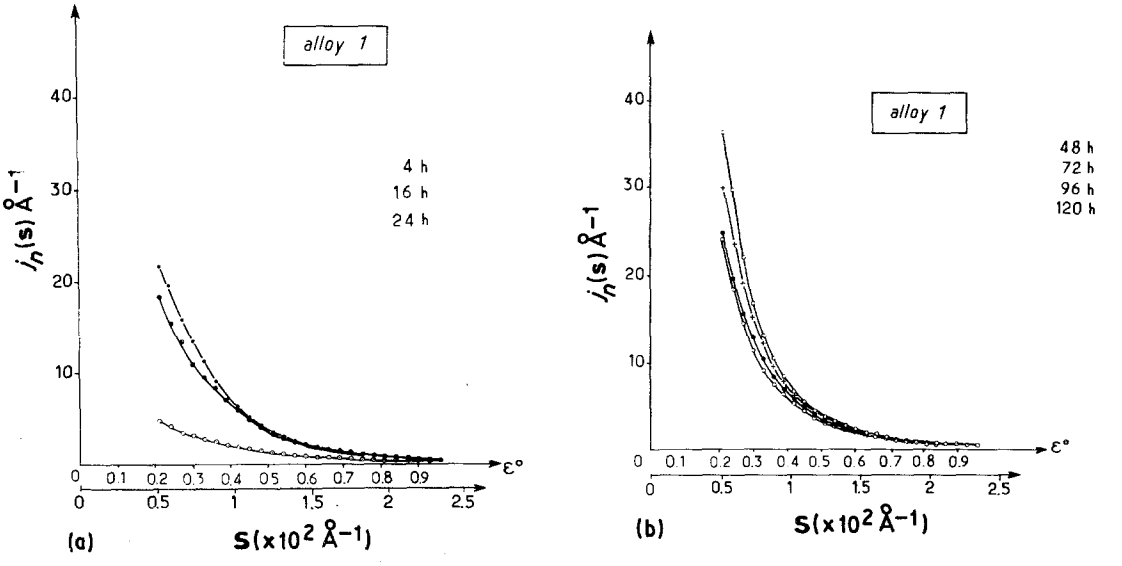

Figure 12 (a) and (b) Small angle X-ray scattering curves $j_n(s)$ as a function of s for Alloy 1.

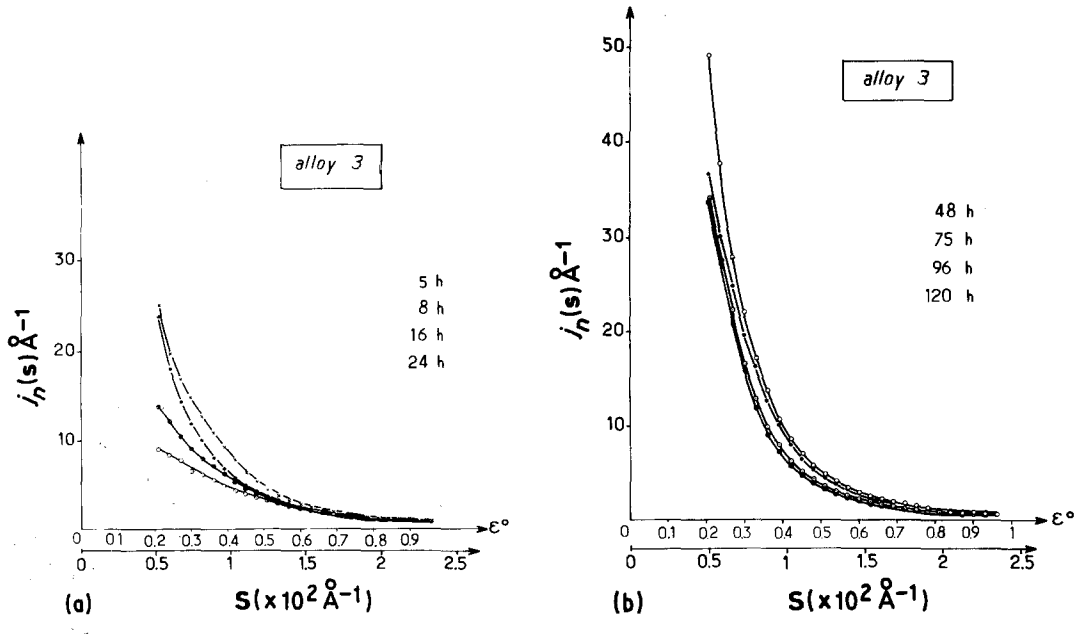

Figure 13 (a) and (b) Small angle X-ray scattering curves $i_n(s)$ as a function of s for Alloy 3.

the ellipsoid which is parallel to the direction ⟨1 1 1⟩ of the martensite. Comparison of Tables I and II indicates that the dimensions of largest precipitates obtained from the scattering curves are distinctly inferior to those measured on the dark-field electron micrographs. This result agrees fairly well with the fact that the gyration radius calculated from the greatest slope of the curve $\log i_n(s) = f(s^2)$ is smaller than that of largest precipitate.

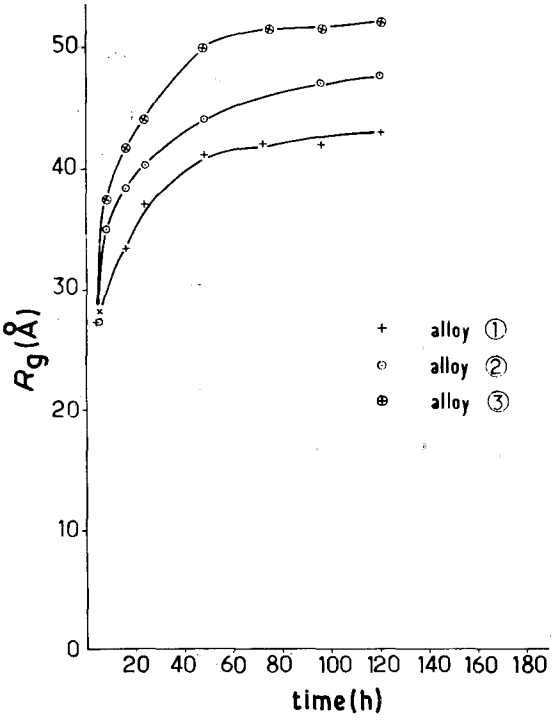

Figure 14 Variations of R_g against time for Alloys 1, 2 and 3.

3.6. Porod's law

In the case of the three alloys studied, for different ageing times at 450° C, it can be said that Porod's law (constant product of $i_n(s)s^3$, assuming a linear and infinite collimation of the X-ray beam) is well verified. This result confirms the fact that our precipitates have (a) on the one hand, an electron density which is distinctly different from that of the martensitic; taking into consideration their structure, of the type A_3W, determined by the electron microscope, their electron density could be estimated between 3.39 and 3.52 electrons Å^{-3}: these two values correspond to the two extreme cases where A represents a mixture of Fe, Ni, Co which can be very rich in Fe (and hence poor in Co + Ni), or inversely one very rich in Ni (and consequently poor in Fe + Co) and (b) on the other hand, the precipitates have rather a globular form. This means that no direction can be neglected with respect to any other and similarly with respect to 1/s. In fact, in the case of rod-shaped precipitates (with a diameter which is very small compared with the value $2H$ = rod length) and cylinders or plate discs of radius R and length

TABLE II

t(h)	R_g (Å)	ν	R_G (Å)	$2R_G$ (Å)	$2\nu R_G$ (Å)
5	28.2	3.6	16.3	33	117
8	37.4	3.7	21.1	42	156
16	41.8	3.9	22.5	45	176
24	44.1	4.1	22.7	46	186
48	50	4.3	24.7	49	211
75	51.5	5.1	21.8	43	219
96	51.9	5.4	20.8	41	221
120	52.3	5.5	20.6	41	226

or thickness $2H$, Porod's law is no longer verified for the same power of s [11].

Figs 15 and 16 indicate the variation of Porod's constant K as a function of increasing ageing time for Alloys 1 and 3. This constant can be expressed as follows

$$j_n(s) \cdot s^3 = \left(\frac{1}{16\pi^2}\right)\left[\frac{(\rho-\rho_0)^2}{\bar{\rho}}\right]\left(\frac{S}{V}\right), \quad (5)$$

where ρ, ρ_0 and $\bar{\rho}$ represent the electronic densities of the precipitates, the matrix and the average electronic density of the alloy, respectively. The ratio S/V is equal to the specific surface of the precipitates,

For Alloys 1, 2, and 3, ρ is constant and is equal to the electronic density of the precipitates A_3W. During ageing, ρ_0 varies between $\bar{\rho}$ and the electronic density of a matrix in which all the content of W of the alloy is found localized in the precipitates. As shown in Table III, ρ_0 varies slowly during ageing and hence the variation of K is strongly influenced by that of the ratio S/V.

In Fig. 15, K increases rapidly during the first hours of ageing, then very slowly up to 120 h. However, up to 120 h there is no coalescence of the precipitates (which will lead to a notable fall in K, and an increase in the gyration radius). For Alloy 3, the slow evolution of K is observed from ageing times less than that indicated in the case of the Alloy 1. Moreover, for the same ageing times, the value of K obtained in the case of Alloy 3 is somewhat greater than that calculated for Alloy 1. This fact can be related to the more important quantity of precipitates in Alloy 3 as shown in Fig. 5c and Fig. 11.

3.7. Evolution of the integral intensity $Q_0 = 2\pi \int_0^\infty s j_n(s)\, ds$

Fig. 17 shows the evolution of Q_0 as a function of ageing time for the three alloys. It is noticed that (a) for an alloy, the increase in Q_0 is firstly rapid during the first hours of ageing, then it becomes slower up to 120 h: this agrees with the precipitate dimensions obtained by X-ray scattering; (b) for the same ageing time, Q_0 increases with increasing weight percentage of W in the alloy: this fact is similarly in good agreement with the evolution of the dimension of the scattering precipitates as the W content increases.

The Q_0 evolution takes into consideration the fact that the reversed austenite for the three alloys

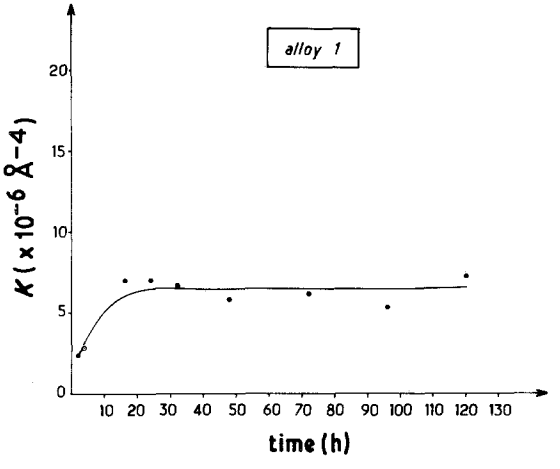

Figure 15 Variation of K against time for Alloy 1.

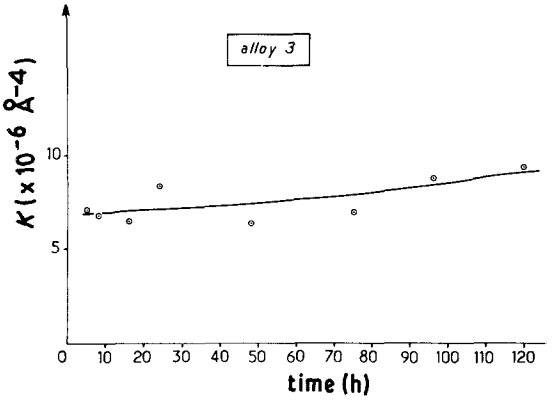

Figure 16 Variation of K against time for Alloy 3.

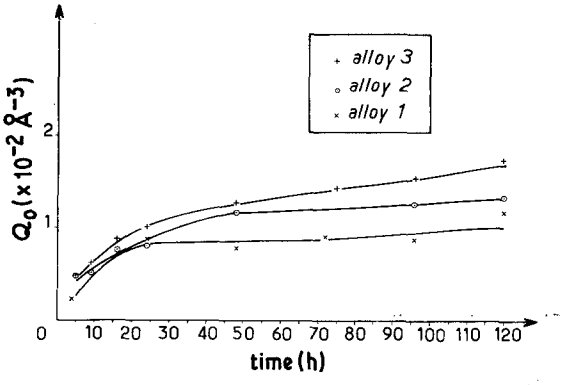

Figure 17 Variation of Q_0 against time for Alloys 1, 2, and 3.

aged at the temperature of 450° C is formed after 120 h.

4. Conclusion

In the case of quaternary alloys of maraging Fe–Ni–Co–W type of 100% lath martensitic structure, whose W content increases up to 10 wt% (solubility limit of W in the martensite), the ageing effect can be observed in three successive stages. Contrary to the quaternary alloys of the same composition, with W-content substituted by Mo, no stage other than the three above-mentioned stages corresponds to the formation of the ω-phase.

In the course of the second stage with which a substantial increase in hardness is associated, there is formation and growth of intermetallic precipitates of A_3W composition (A is a mixture of Fe, Ni and/or Co) of orthorhombic structure with the parameters: $a = (0.508 \pm 0.01)$ nm, $b = (0.415 \pm 0.01)$ nm and $c = (0.425 \pm 0.1)$ nm.

These precipitates are ellipsoidals, elongated to some tens of nm, whose direction of growth is $\langle 1\,1\,1 \rangle$ of the martensitic matrix. Their orientation relationship with this matrix is as follows

$$\{0\,1\,1\}_M // (0\,1\,0)_{A_3W}$$

$$\langle 1\,\bar{1}\,1 \rangle_M // [1\,0\,0]_{A_3W}.$$

TABLE III

Alloy	$\bar{\rho} = \rho_0$ ($t = 0$ electrons Å^{-3})	ρ_0 ($t = \infty$ electrons Å^{-3})
1	2.30	2.23
2	2.34	2.22
3	2.37	2.22

In terms of the mechanical properties (taking into account the hardness measurements), these alloys seem to be less interesting than those of Mo.

The demi-coherence of the A_3W precipitates with the martensite does not assist the production of a hardness as great as that associated with the superstructure formation or the ω-phase.

References

1. J. BOURGEOT, P. MAITREPIERRE, J. MANENC and B. THOMAS, Fifth International Symposium, University of California, Berkeley, California (1971).
2. C. SERVANT, Thèse de Doctorat ès-Sciences, Université Paris Sud, Orsay (1972).
3. A. F. YEDNERAL and M. D. PERKAS, *Fiz. Metal. Metalloved* **33** (1972) 315.
4. C. SERVANT, G. MAEDER and P. LACOMBE, *Met. Trans.* **6A** (1975) 981.
5. A. AGNEL, F. HEDIN, G. MAEDER, C. SERVANT and P. LACOMBE, *Acta Met.* **25** (1977) 1445.
6. K. SHIMIZU and H. OKAMOTA, *Trans. Japan Inst. Met.* **12** (1971) 273.
7. W. R. BANDI, J. L. INTZ and L. M. MELNICK, *J. Iron Steel Inst.* **207** (1969) 348.
8. C. SERVANT, G. MAEDER and P. LACOMBE, *Met. Trans.* **10A** (1979) 1607.
9. C. SERVANT, P. LACOMBE and M. GRIVEAU, *J. Mater. Sci.* **15** (1980) 859.
10. G. MAEDER, Thèse de Doctorat ès-Sciences, Université de Paris-Sud, Orsay (1975).
11. A. GUINIER and G. FOURNET, "Small angle scattering of X-rays", (Wiley, New York, 1955).
12. J. BURKE, "La cinétique des changements de phase dans les métaux", (Masson Edit, Paris, 1968).
13. P. L. GRUZIN, *Dokl. Akad. Nauk.* **94** (1954) 81

Received 12 June and accepted 18 July 1980.